nature chemistry

ARTICLES

PUBLISHED ONLINE: 5 SEPTEMBER 2010 | DOI: 10.1038/NCHEM.825

Spectroscopic visualization of sound-induced liquid vibrations using a supramolecular nanofibre

Akihiko Tsuda[1]*, Yuka Nagamine[2], Reiko Watanabe[2], Yoshiki Nagatani[3], Noriyuki Ishii[4] and Takuzo Aida[2]*

The question of whether sound vibration of a medium can bring about any kind of molecular or macromolecular events is a long-standing scientific controversy. Although it is known that ultrasonic vibrations with frequencies of more than 1 MHz are able to align certain macromolecules in solution, no effect has yet been reported with audible sound, the frequency of which is much lower (20–20,000 Hz). Here, we report on the design of a supramolecular nanofibre that in solution becomes preferentially aligned parallel to the propagation direction of audible sound. This phenomenon can be used to spectroscopically visualize sound-induced vibrations in liquids and may find application in a wide range of vibration sensing technologies.

Sound is vibration and can therefore have a range of frequencies. It can be transmitted through all forms of matter, whether gas, liquid, solid or plasma[1]. Many organisms, including humans, can sense oscillations in matter; ears respond by triggering various chemical and biomolecular events. It has also been reported that the taste of alcoholic beverages such as wine and distilled spirits can change following an acoustic aging process[2], and an empirical technique based on this concept has been developed by the industry. However, the question of whether the vibration of a medium upon sound irradiation can cause any kind of molecular or macromolecular events remains controversial.

Surface acoustic waves with frequencies of 1–100 MHz have been used in a technique for the actuation of fluids, microscale patterning of polymers and manipulation of microparticles on surfaces[3–5]. Solutions containing anisotropic macroscopic objects such as polymers and colloidal particles have also been reported to exhibit ultrasonically induced birefringence[6–10]. The timescale of ultrasonic vibrations (>1 MHz) allows the formation of a microscopic velocity gradient or radiation pressure for macromolecules in solution, inducing them to become aligned[10]. However, the alignment of macromolecules using audible sound, the frequency of which is much lower (20–20,000 Hz) than that of ultrasonic waves[1], has not been reported. This is probably due to the fact that the wavelength of audible sound is much longer than molecular length-scales. For example, the wavelengths of an audible sound with a frequency of 100 Hz and an ultrasonic sound with a frequency of 1 MHz, in water, are ~15 m and 1.5 mm, respectively.

We have previously reported that a supramolecular polymer comprising *J*-aggregated zinc porphyrin dendrimers can be used to chiroptically visualize the macroscopic chirality of a vortex generated by mechanical rotary stirring of a fluid in a cuvette[11–13]. The sign of the circular dichroism (CD) response changes quickly upon reversal of the stirring direction. The observed chiroptical activity is probably due to a macroscopic helical alignment of nanofibres in the torsional flows of the vortex. This finding prompted us to attempt the visualization of sound-induced liquid vibrations using a supramolecular nanofibre[14,15]. In the present study, we demonstrate that a newly designed nanofibre, the supramoleculary polymerized zinc porphyrin **1**, can be acoustically aligned in solution.

Results

We synthesized zinc porphyrin **1** (which bears a 4-pyridyl group and two 4-carboxyphenyl groups) with the expectation that cyclic tetramerization would occur due to zinc–pyridyl coordination[16–20], followed by polymerization via hydrogen-bonding interactions of carboxyphenyl groups on adjacent tetramers, thus forming the supramolecular nanofibre $\mathbf{1}_{\mathbf{poly}}$ (Fig. 1)[21–26]. Solid samples of **1** were barely soluble in low-polar solvents, but homogeneous solutions were obtained upon sonication for 30 s. Although the absorption spectrum of **1** in toluene or benzene gradually decreased in intensity due to the formation of a precipitate, no significant changes occurred with time in $CHCl_3$.

Dynamic light scattering (DLS) analysis showed that a solution of **1** in $CHCl_3$ (concentration, 4.0×10^{-5} M at 20 °C) contained self-assembled nano-objects with lengths ranging from 425 to 1,143 nm and an average radius of 667 nm (Supplementary Fig. S1). Scanning electron microscopy (SEM) performed on a solution of self-assembled **1** in $CHCl_3$ (4.0×10^{-6} M), following air-drying, revealed the formation of linear nanofibres with an extremely high aspect ratio (Fig. 2a). Transmission electron microscopy (TEM) demonstrated that these fibres were straight, with no branched structures (Fig. 2b). Because the thinnest fibres in the TEM images were 3–4 nm thick, corresponding to the diameter of a molecular model of the cyclic tetramer of **1**, the larger-diameter nanofibres, observed using both SEM and TEM, are probably bundles of $\mathbf{1}_{\mathbf{poly}}$.

Because the polymeric assembly of **1** gave broad ^{1}H nuclear magnetic resonance (NMR) signals in $CDCl_3$, we synthesized a reference compound **2** bearing only one carboxyphenyl group, with the expectation that a box-shaped assembly comprising eight units of **2** ($\mathbf{2}_8$) would be formed in a manner analogous to that observed

[1]Department of Chemistry, Graduate School of Science, Kobe University, 1-1 Rokkodai-cho, Nada-ku, Kobe 657-8501, Japan, [2]Department of Chemistry and Biotechnology, School of Engineering and Center for NanoBio Integration, The University of Tokyo, 7-3-1 Hongo, Bunkyo-ku, Tokyo 113-8656, Japan, [3]Department of Electronic Engineering, Kobe City Collage of Technology, 8-3 Gakuen-Higashi-machi, Nishi-ku, Kobe 651-2194, Japan, [4]Biological Information Research Center, National Institute of Advanced Industrial Science and Technology (AIST), Tsukuba Central-6, 1-1-1 Higashi, Tsukuba, Ibaraki 305-8566, Japan. *e-mail: tsuda@harbor.kobe-u.ac.jp; aida@macro.t.u-tokyo.ac.jp

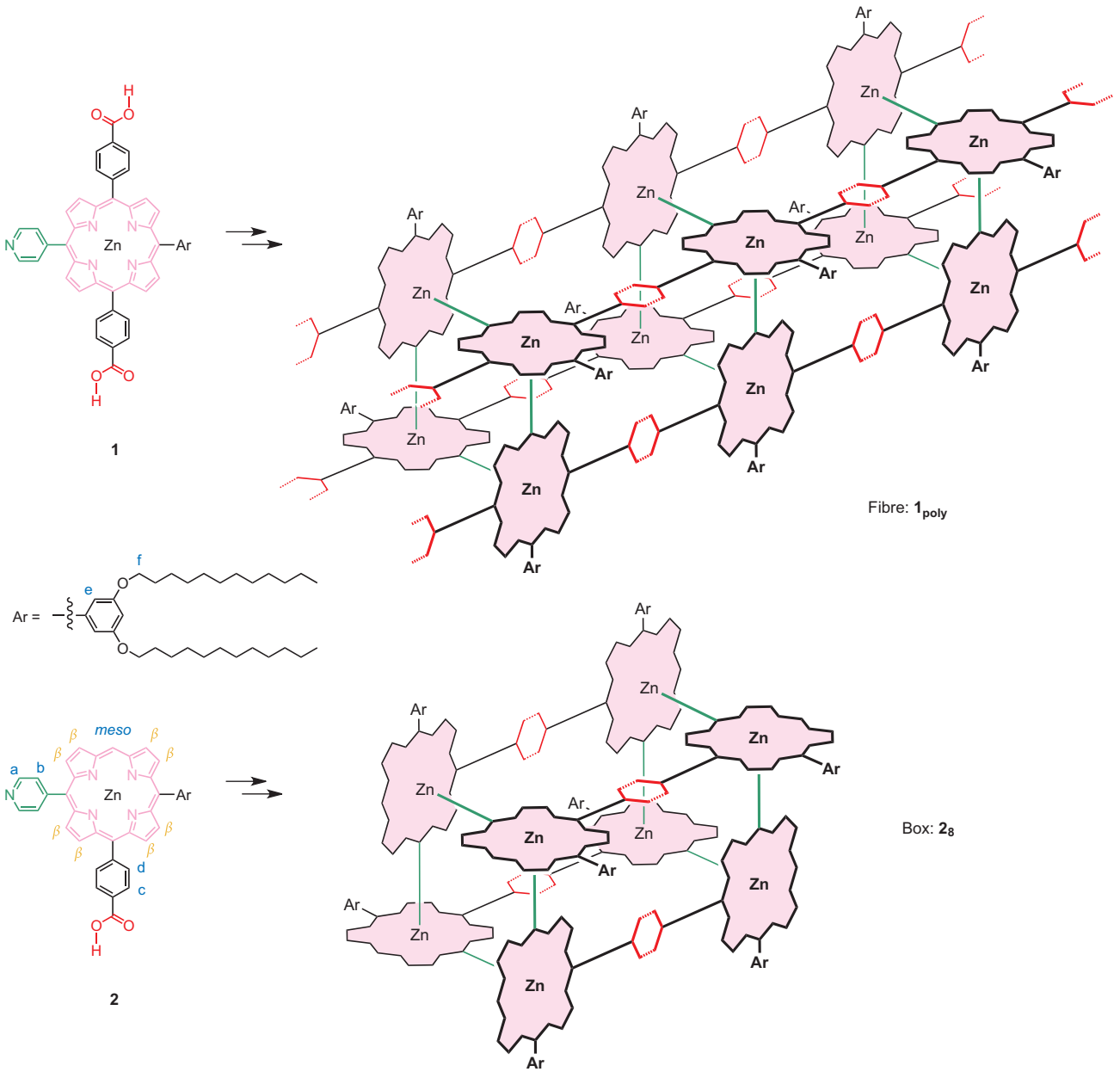

Figure 1 | Zinc porphyrin derivatives for self-assembly. Molecular structures of zinc porphyrin **1** and a reference compound **2**, both bearing 4-pyridyl and 4-carboxyphenyl groups, and their self-assembled structures formed by coordination and hydrogen-bonding interactions. Labels a–f, *meso* and β on **2** indicate the hydrogen atoms labelled in the ^{1}H NMR spectra in Fig. 3.

for the self-assembly of **1** (Fig. 1). The ^{1}H NMR spectrum of **2** in $CDCl_3$ provided a spectral pattern characteristic of previously reported box-shaped zinc porphyrin assemblies (Fig. 3a, I)[17,19,20]. In comparison with the spectrum for monomeric **2**, which is formed in the presence of 2% pyridine (Fig. 3a, III), the proton signals of H^a and H^b of the pyridyl group (Fig. 1), which favours a perpendicular orientation with respect to the porphyrin plane, have dramatically large upfield shifts in $\mathbf{2_8}$ due to the ring-current effect of the porphyrin ring. These signals are further split under the influence of the different magnetic environments inside and outside the box-shaped architecture. Similar splittings were also observed for H^c, H^d and H^e in the other aromatic substituents, and also for H^f of the 3,5-didodecyloxy groups. The *meso*- and pyrrole-β protons of the porphyrin ring give rise to one singlet signal and eight doublet signals, respectively. The proton signal of the carboxyl group appeared at 14.37 ppm at –50 °C.

The cyclic tetramer of **2** ($\mathbf{2_4}$), a possible intermediate of $\mathbf{2_8}$, could be isolated spectroscopically following the addition of deuterated acetic acid (2%), which selectively breaks the hydrogen bonding between adjacent carboxyl groups (Fig. 3a, II). The corresponding ^{1}H NMR spectrum showed eight pyrrole-β signals and broadened, upfield-shifted pyridyl signals, the pattern of which is rather similar to that of the cyclic tetramer of a methylester version of **2** (Supplementary Fig. S2). These spectral features indicate that the heterogeneous interactions of coordination and hydrogen bonds occur separately in the construction of the box-shaped architecture[27,28]. Consequently, it is probable that these interactions also occur separately in the supramolecular polymeric system composed of **1**.

Orientation of the nanofibres of **1** in solution can be characterized using linear dichroism (LD) spectroscopy[12,13,29–31]. The LD spectrometer was equipped with a 12 × 12 × 45 mm optical

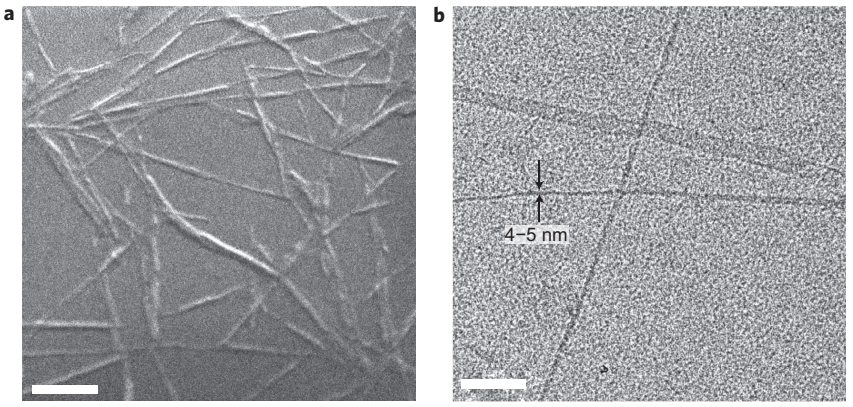

Figure 2 | Electron micrographs of self-assembled nanofibres formed from zinc porphyrin 1. a, SEM micrograph of an air-dried sample of self-assembled **1** in $CHCl_3$ solution (4.0×10^{-6} M) deposited on a silicon substrate. Scale bar, 300 nm. **b**, TEM micrograph of an identical air-dried sample deposited on a specimen grid covered with a thin carbon support film. Scale bar, 100 nm.

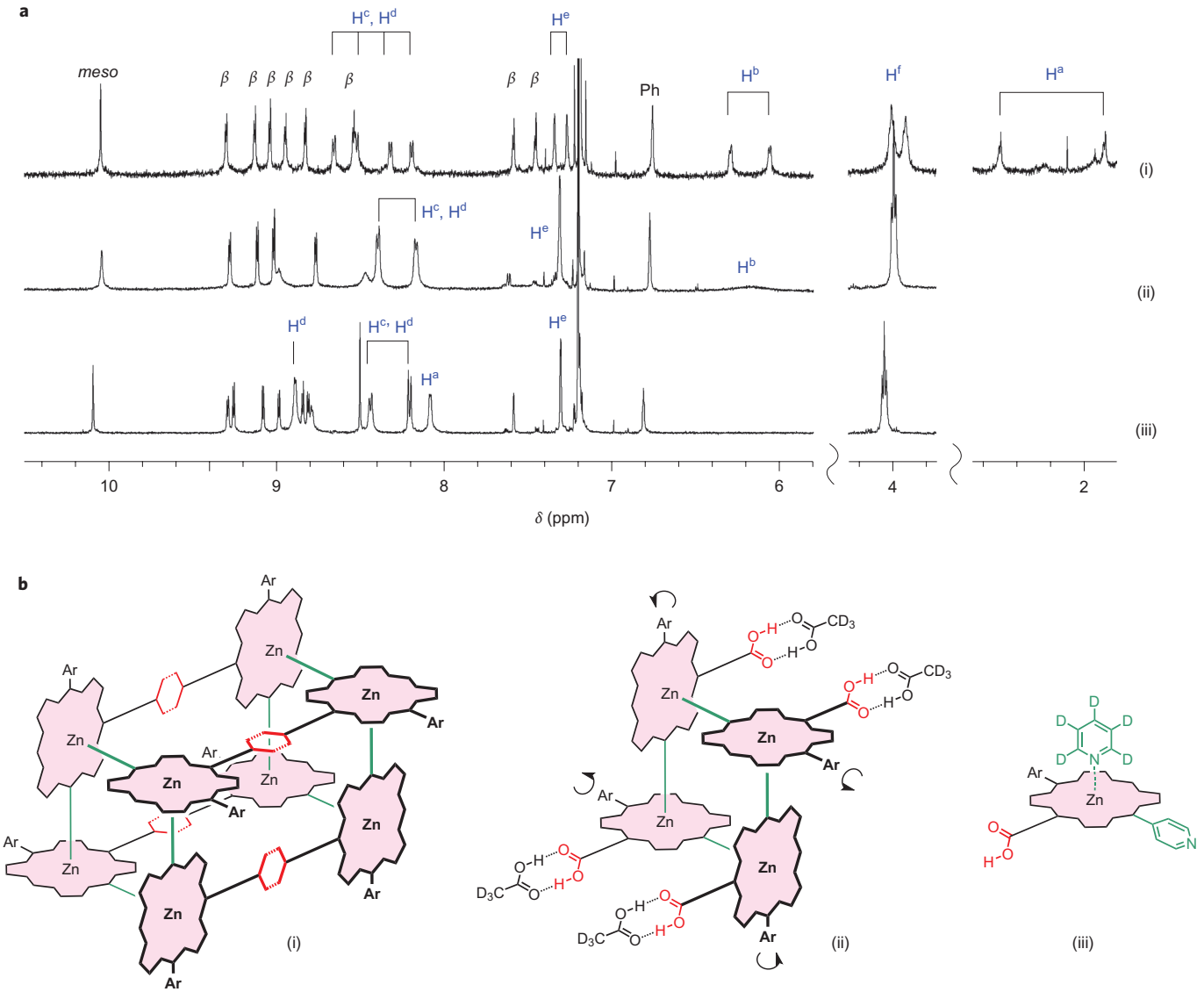

Figure 3 | ^{1}H NMR spectra of self-assembled zinc porphyrin 2. a, ^{1}H NMR spectra of **2** at 20 °C in $CDCl_3$ (i), $CDCl_3/CD_3CO_2D$ (98:2) (ii) and $CDCl_3$/pyridine-d_5 (98:2) (iii). **b**, Schematic of self-assembled structures of **2**, as deduced from the ^{1}H NMR profiles of (i), (ii) and (iii) in **a**.

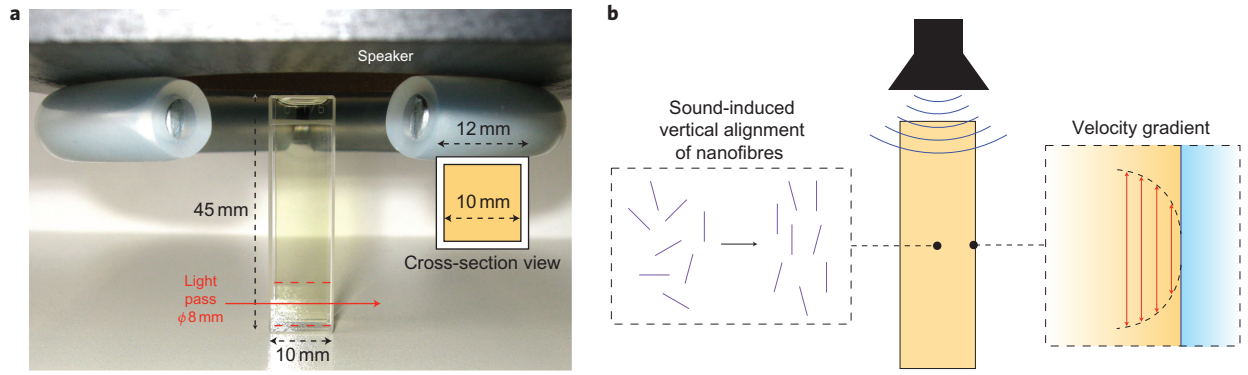

Figure 4 | Effect of liquid vibrations generated by sound irradiation on the alignment of nanofibres. a, A sample solution is exposed to sound irradiation in a 12 × 12 × 45 mm (outer dimensions) quartz optical cuvette constructed from 1-mm-thick glass panels. For LD spectroscopy, an 8.0-mm-diameter beam of linearly polarized light was passed through the sample solution at a position 4 mm above the bottom inner surface of the cuvette. A loudspeaker with a diameter of 70 mm was located 20 mm above the cuvette. **b**, Schematic of the vertical alignment of nanofibres induced by sound vibration (left) and the resulting velocity gradient between the centre and sidewalls of the cuvette (right).

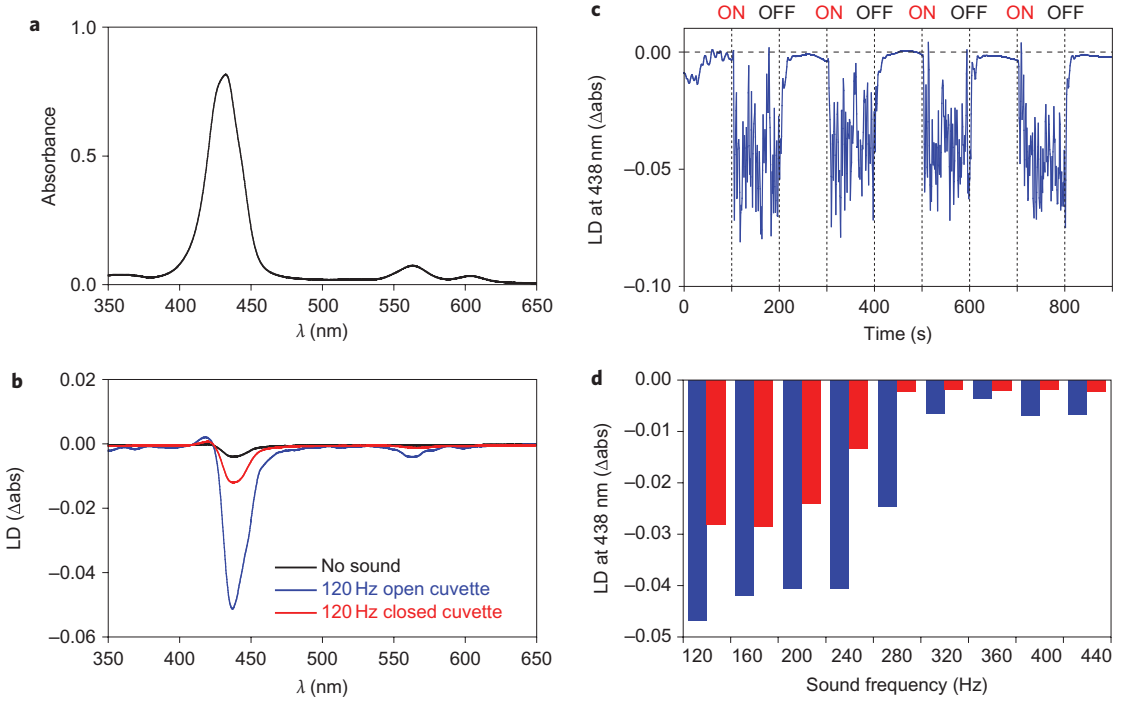

Figure 5 | Spectroscopic visualization of sound-induced liquid vibrations with self-assembled 1. a, Absorption spectrum of a solution of **1** in $CHCl_3$ (4.0×10^{-6} M) at 20 °C. **b**, LD spectra of the same solution at 20 °C contained in a 10 × 10 × 45 mm quartz optical cuvette, with and without sound irradiation at 120 Hz (blue and black curves, respectively), and contained in a closed cuvette with a 12 × 12 × 2 mm^3 Teflon-coated plastic cap with sound irradiation of 120 Hz (red curve). The sound pressure level at 120 Hz was measured as 31.6 Pa at the top of the cuvette. **c**, Change in LD intensity at 438 nm in response to a repeated ON–OFF sequence of 120 Hz sound irradiation at 20 °C. **d**, Changes in LD intensity at 438 nm and 20 °C in response to different sound frequencies for applied voltages of 10 V (blue bars) and 5 V (red bars) on the function generator. The LD intensities were averaged over 30 s.

cuvette constructed from 1-mm-thick quartz glass panels, which was filled with a $CHCl_3$ solution of **1** (4.0×10^{-6} M) (Fig. 4a). The cuvette was fixed in a steel holder in the spectrometer. The LD responses were monitored 40 mm below the top of the optical cuvette using an 8.0-mm-diameter beam of linearly polarized light. A sinusoidal wave, produced by a function generator, was intensified using an amplifier to produce audible sound of variable frequency, which was emitted from a loudspeaker (diameter, 70 mm; Supplementary Figs S3 and S4) located 20 mm above the top of the cuvette. The sound pressure varied with frequency (1,000–100 Hz) in the range 18.9–31.6 Pa, and was essentially constant in the central area (diameter, 30–40 mm) of the speaker. No deformation of the sinusoidal wave pattern was observed at this position. The output wave voltage was proportional to the applied voltage of the function generator.

The solution displayed a weak LD response in the absence of audible sound, probably due to convection flows caused by a difference in temperature between the surface and bottom of the solution (Fig. 5b, black curve)[13]. However, a strong LD response was obtained upon irradiation with audible sound in the frequency range 280–100 Hz, corresponding to a sound pressure of 16.6–31.6 Pa (Fig. 5b, blue curve). For example, when the solution was irradiated with sound of 120 Hz (31.6 Pa), intense LD bands were observed at both the Soret absorption band (Fig. 5a,b; 418 nm ($\Delta abs = 0.0022$) and 437 nm

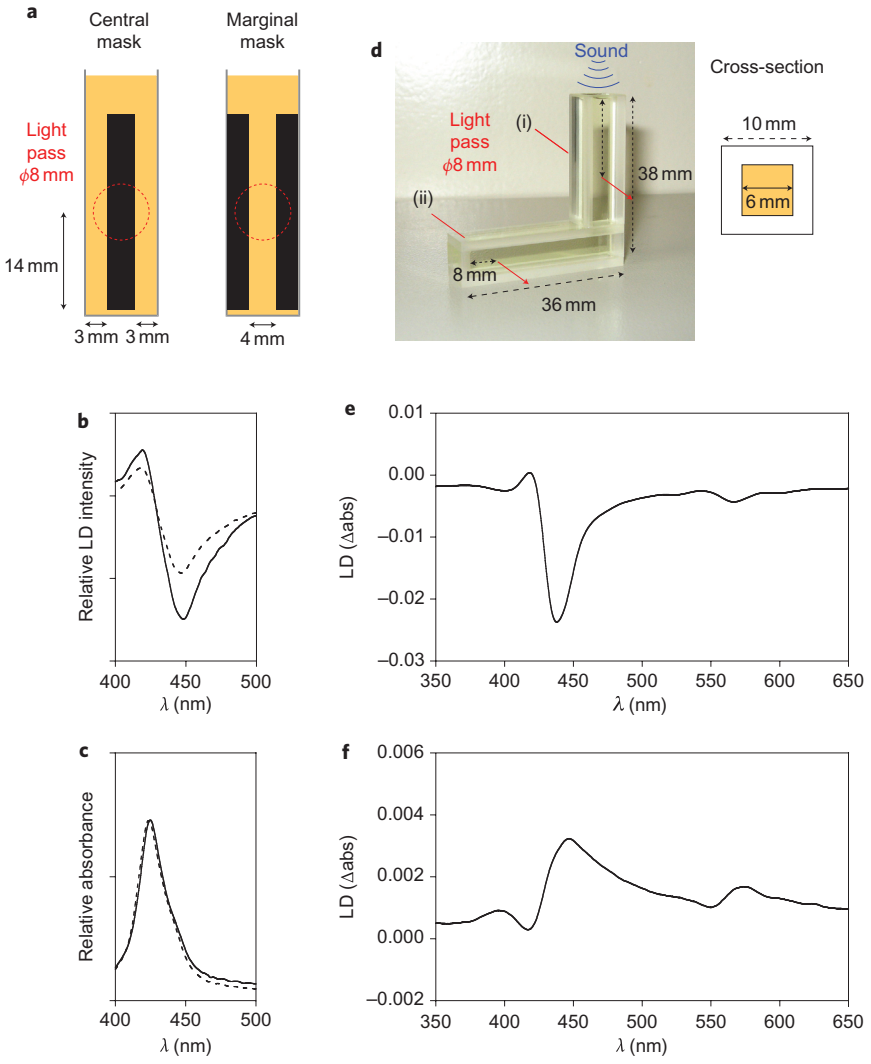

Figure 6 | Pointwise spectroscopic visualization of sound-induced liquid vibrations in masked cuvettes and an L-shaped cuvette containing a solution of self-assembled 1. a, Quartz optical cuvettes ($12 \times 12 \times 45$ mm^3) masked vertically through the centre with 4-mm-wide black tape (left) and at the margins with 3-mm-wide black tape to leave a 4-mm-wide central slit (right). **b**,**c**, Relative LD intensity (**b**) and relative absorbance (**c**) of a $CHCl_3$ solution of **1** (4.0×10^{-6} M) at 20 °C with the cuvettes masked in the central and marginal sections (solid and dashed curves, respectively) upon sound irradiation with 120 Hz. **d**, An L-shaped cuvette with vertical and horizontal sections of length 40 mm, a cross-section of 10×10 mm^2 and glass thickness of 2 mm. **e**,**f**, LD spectra for a $CHCl_3$ solution of **1** (4.0×10^{-6} M) contained in the L-shaped cuvette at 20 °C are shown for position (i) (**e**), located 20 mm from the top of the cuvette, and for position (ii) (**f**), located in the horizontal section of the cuvette 25 mm from the centre of the vertical section.

($\Delta abs = -0.0512$)) and the Q-band (563 nm ($\Delta abs = -0.0039$) and 577 nm ($\Delta abs = -0.0018$)). When irradiation was halted, LD activity in the solution stopped immediately, with a half-life of ~5 s. Although an analogous LD spectrum could be induced by directly shaking the sample solution, generating long-lived liquid oscillations, the lifetime of the induced signals following shaking was much longer, with a half-life of 30 s (Supplementary Fig. S5). The acoustic LD response was dramatically reduced on insertion of a $12 \times 12 \times 2$ mm Teflon-coated plastic cap at the top of the cuvette (Fig. 5b, red curve). Solutions containing reference samples of non-assembled **1** in $CHCl_3$/pyridine (98:2) and the box-shaped assembly $\mathbf{2_8}$ in $CHCl_3$ gave no LD response upon sound irradiation.

These results show that nanofibres of **1** in solution respond significantly to acoustic vibrations translated from aerial vibrations generated by an audio speaker. Because there is little propagation of sound waves from gas to liquid phases due to their extremely different acoustic impedances, the nanofibres must therefore sense extremely weak induced vibrations of the liquid media. In fact, macroscopic fluctuations of the larger aggregates of $\mathbf{1_{poly}}$ in $CHCl_3$, induced by sound irradiation at 120 Hz, could be observed visually as perturbations in the scattering of laser light passing through the solution, showing the Tindal phenomenon at higher concentrations of **1** (Supplementary Video S1).

To assess this intriguing LD effect, $\mathbf{1_{poly}}$ in a $CHCl_3$ solution (4.0×10^{-5} M) was dip-coated onto a 0.12–0.17-mm-thick glass plate[12,13]. The dip-coated thin film, in which the nanofibres were preferentially oriented along the dipping direction, showed a virtually identical LD spectral pattern to that obtained for the solution described above (Supplementary Fig. S6, solid curve). As expected, the spectral signals were inverted following a 90° rotation of the sample relative to the vertical axis of the linearly polarized light beam passing through the sample in the LD spectroscopy setup (Supplementary Fig. S6, dashed curve). Thus, it can be concluded that the nanofibres in a solution of $CHCl_3$ predominantly adopt a vertical orientation, parallel to the propagation direction of the irradiated sound (Fig. 4b).

When monitoring the LD response of the above solution of **1** in $CHCl_3$ at 438 nm, and repeatedly turning the sound (120 Hz,

31.6 Pa) on and off, the nanofibres were seen to respond quickly to the induced liquid vibrations (Fig. 5c). The LD response was highly dependent on the frequency and amplitude of the sound (Fig. 5d). Application of sound with frequencies below 280 Hz (pressures in the range 21.6–31.6 Pa) led to LD induction, with a maximum value of Δabs (−0.047) achieved at 100 Hz (28.4 Pa). In contrast, no LD response was observed upon sound irradiation with frequencies in the range 320–1,000 Hz (18.9–21.4 Pa). When sound of approximately half the pressure, and hence a weaker vibrational strength, was applied to the sample solution, an LD response of lower but still significant intensity was induced at frequencies of less than 240 Hz (Fig. 5d, red bars). Because low-frequency sound corresponds to a slow directional change in the liquid vibrations, the resulting large fluctuations in the solvent may allow alignment of the supramolecular nanofibres. Low-frequency sound is less directional, and thus easily disperses in air. Consequently, when the solution surface was lowered by partially emptying the solution from the cuvette, the LD intensity dramatically decreased (Supplementary Fig. S7).

To investigate the manner in which sound propagated in the supramolecular nanofibre solution, we performed spectroscopic visualizations of local liquid vibrations with the cuvettes selectively masked vertically over their central or marginal sections (Fig. 6a) and with an L-shaped cuvette (Fig. 6d). Interestingly, the LD intensity observed through the central slit (for the cuvette masked along the margins) was smaller than that observed through the marginal parts (for the cuvette masked through its centre) (Fig. 6b), despite there being no notable changes in the corresponding absorption spectra (Fig. 6c)[12]. These observations suggest preferential alignment of the nanofibres flowing around the sidewall of the cuvette. This result suggests possible visualizations of local vibrations of acoustic liquids with qualitative as well as quantitative insights. We then carried out a spectroscopic visualization of the sound-induced local liquid vibration in an L-shaped cuvette. Because lower-frequency sound is poorly directional, we expected a possible propagation of the sound vibration to the end of the horizontal section of the L-shaped cuvette via its square corner. As was also observed for the straight cuvette, a negative LD response at 438 nm (Fig. 6e) was obtained at a position 20 mm below the solution surface (position (i) in Fig. 6d). In sharp contrast, a weak LD response with a positive sign (Fig. 6f) emerged in the horizontal branch of the cuvette, at position (ii) in Fig. 6d. The nanofibres are thus able to sense weak horizontal vibrations associated with the propagation of low-frequency sound over long distances in the solution, including a directional change of 90°.

Discussion

When considering the mechanism of sound-induced alignment of nanofibres in solution, it should be noted that the wavelength of the audible sound is far longer than the length of the cuvette (for example, the wavelength is 8.3 m in the liquid phase for a frequency of 120 Hz at 25 °C). The sound, which can be considered as periodic cycles of compaction and expansion of air, will act on the sample solution in the form of a periodic increase and decrease of atmospheric pressure, respectively. This will induce a periodic change in the volume of the sample solution and give rise to vibrations, causing the solvent molecules to move parallel to the glass walls of the cuvette. Because such fluidic behaviour gives rise to a velocity gradient in the solution between the sidewalls and the centre of the cuvette (Fig. 4b)[32], physical friction can cause the nanofibres to align hydrodynamically, becoming oriented parallel to the direction of liquid vibration, as observed for the dip-coated film[12,13]. Because a large hydrodynamic gradient must occur in the boundary layer of the liquid flowing around the wall surface[32], the larger LD intensity observed at the sidewall of the cuvette in the pointwise LD spectroscopy (Fig. 6b) is a quite reasonable consequence of this mechanism.

In the present study, we have successfully carried out the spectroscopic visualization of liquid vibrations induced by irradiation with audible sound, using a supramolecular nanofibre formed by the self-assembly of **1**. The nanofibres align parallel to the direction of sound propagation as a result of hydrodynamic interaction of $\mathbf{1}_{\mathbf{poly}}$ with the solvent molecules. The observed phenomenon is probably a general unique function of linear supramolecular nanofibres, because the previously developed supramolecular polymer of dendritic zinc porphyrin was also shown to exhibit an analogous characteristic, although at higher concentrations (Supplementary Fig. S8)[11,12]. However, in controlled experiments, no acoustic LD responses were observed for solutions of conjugated polymers such as a directly linked polyporphyrin, which has a long rod-shaped structure[33], and polystyrene, which allows ultrasonically induced birefringence[10]. The high sensitivity of $\mathbf{1}_{\mathbf{poly}}$ to liquid vibrations is very attractive for sensing applications involving a range of vibrations.

Methods

Most of the reagents and solvents were used as received from commercial sources without further purification. For column chromatography, Wakogel C-300HG (particle size, 40–60 mm, silica), C-400HG (particle size, 20–40 mm, silica), aluminium oxide 90 standardized (Merck) and Bio-Beads S-X1 (BIO RAD) were used.

LD spectra were recorded using a JASCO type J-820 spectropolarimeter equipped with a JASCO type PTC-423L temperature/stirring controller and a custom-made sound generator. The latter was composed of a digital function generator (NF model DF1906), an integral amplifier (DENON model PMA-390AE) and a sound speaker (AURA Sound model NS3-193-4A). Sound pressure was recorded using a condenser microphone (Brüel & Kjaer type 4135) equipped with a measuring amplifier (Brüel & Kjaer type 2610) and an oscilloscope (Tektronix model TDS1001B) in an anechoic room. Absorption spectra were recorded using a JASCO type V-670 UV/VIS/NIR spectrometer equipped with a JASCO type ETC-717 temperature/stirring controller. Before carrying out spectral measurements, sample solutions of $\mathbf{1}_{\mathbf{poly}}$ ($[\mathbf{1}] = 4.0 \times 10^{-6}$ M) in $CHCl_3$ were prepared by sonication of the initial suspension for 10 s, which was then allowed to stand in the dark at 20 °C for 10 min. ^{1}H NMR spectra were recorded using a JEOL model EX-270 or GSX-500 spectrometer, where the chemical shifts (δ in ppm) were determined with respect to tetramethylsilane (TMS) as an internal standard. Matrix-assisted laser desorption/ionization time-of-flight mass spectrometry (MALDI-TOF-MS) was performed using a 9-nitroanthracene matrix on an Applied Biosystems BioSpectrometry Workstation model Voyager-DE STR spectrometer. DLS measurements were performed using an Otsuka model ELS-Z2 instrument. TEM images were recorded using a Philips model Tecnai F20 transmission electron microscope operating at 120 kV. SEM imaging was performed using a JEOL model JSM–6700F FE–SEM operating at 5 kV. The laser scattering experiment was performed using a KOKUYO model laser pointer (wavelength, 532 nm) with a maximum output of 1 mW.

Received 13 April 2010; accepted 26 July 2010;
published online 5 September 2010

References

1. Beranek, L. L. *Acoustics* (McGraw-Hill, 1954).
2. Komatsu, A. *Food Science Journal* [in Japanese] **203,** 52–62 (1995).
3. Shilton, R., Tan, M. K., Yeo, L. Y. & Friend, J. R. Particle concentration and mixing in microdrops driven by focused surface acoustic waves. *J. Appl. Phys.* **104,** 014910 (2008).
4. Alvarez, M., Friend, J. R. & Yeo, L. Y. Surface vibration induced spatial ordering of periodic polymer patterns on a substrate. *Langmuir* **24,** 10629–10632 (2008).
5. Friend, J. R., Yeo, L. Y., Arifin, D. R. & Mechler, A. Evaporative self-assembly assisted synthesis of polymeric nanoparticles by surface acoustic wave atomization. *Nanotechnology* **19,** 145301 (2008).
6. Kawamura, H. *Kagaku* [in Japanese] **7,** 6–7 (1938).
7. Lipeles, R. & Kivelson, D. Experimental studies of acoustically induced birefringence. *J. Chem. Phys.* **72,** 6199–6208 (1980).
8. Yasuda, K., Matsuoka, T., Koda, S. & Nomura, H. Dynamics of V_2O_5 sol by measurement of ultrasonically induced birefringence. *Jpn J. Appl. Phys.* **33,** 2901–2904 (1994).
9. Yasuda, K., Matsuoka, T., Koda, S. & Nomura, H. Dynamics of entanglement networks of rodlike micelles studied by measurements of ultrasonically induced birefringence. *J. Phys. Chem. B* **101,** 1138–1141 (1997).
10. Nomura, H., Matsuoka, T. & Koda, S. Ultrasonically induced birefringence in polymer solutions. *Pure Appl. Chem.* **76,** 97–104 (2004).
11. Yamaguchi, T., Kimura, T., Matsuda, H. & Aida, T. Macroscopic spinning chirality memorized in spin-coated films of spatially designed dendritic zinc porphyrin *J*-aggregates. *Angew Chem. Int. Ed.* **43,** 6350–6355 (2004).

12. Tsuda, A. *et al*. Spectroscopic visualization of dynamic vortex flows using a dye-containing nanofiber. *Angew Chem. Int. Ed.* **46,** 8198–8202 (2007).
13. Wolffs, M. *et al*. Macroscopic origin of circular dichroism effects by alignment of self-assembled fibers in solution. *Angew. Chem. Int. Ed.* **46,** 8203–8205 (2007).
14. de Greef, T. F. A. & Meijer, E. W. Supramolecular polymers. *Nature* **453,** 171–173 (2008).
15. Chen, Z., Lohr, A., Saha-Möller, C. R. & Würthner, F. Self-assembled π-stacks of functional dyes in solution: structural and thermodynamic features. *Chem. Soc. Rev.* **38,** 564–584 (2009).
16. Chi, X., Guerin, A. J., Haycock, R. A., Hunter, C. A. & Sarson, L. D. Self-assembly of macrocyclic porphyrin oligomers. *Chem. Commun.* 2567–2568 (1995).
17. Tsuda, A., Nakamura, T., Sakamoto, S., Yamaguchi, K. & Osuka, A. A self-assembled porphyrin box from *meso-meso*-linked bis{5-*p*-pyridyl-15-(3,5-di-octyloxyphenyl)porphyrinato zinc(II)}. *Angew Chem. Int. Ed.* **41,** 2817–2821 (2002).
18. Fukushima, K. *et al*. Synthesis and properties of Rhodium(III) porphyrin cyclic tetramer and cofacial dimer. *Inorg. Chem.* **42,** 3187–3193 (2003).
19. Tsuda, A., Hu, H., Tanaka, R. & Aida, T. Planar or perpendicular? Conformational preferences of π-conjugated metalloporphyrin dimers and trimers in supramolecular tubular arrays. *Angew Chem. Int. Ed.* **44,** 4884–4888 (2005).
20. Aimi, J. *et al*. 'Conformational' solvatochromism: spatial discrimination of nonpolar solvents using a supramolecular box of a π-conjugated zinc bisporphyrin rotamer. *Angew Chem. Int. Ed.* **47,** 5153–5156 (2008).
21. Shi, X., Barkigia, K. M., Fajer, J. & Drain, C. M. Design and synthesis of porphyrins bearing rigid hydrogen bonding motifs: highly versatile building blocks for self-assembly of polymers and discrete arrays. *J. Org. Chem.* **66,** 6513–6522 (2001).
22. Shoji, O., Tanaka, H., Kawai, T. & Kobuke, Y. Single molecule visualization of coordination-assembled porphyrin macrocycles reinforced with covalent linkings. *J. Am. Chem. Soc.* **127,** 8598–8599 (2005).
23. Michelsen, U. & Hunter, C. A. Self-assembled porphyrin polymers. *Angew Chem. Int. Ed.* **39,** 764–767 (2000).
24. Ogawa, K. & Kobuke, Y. Formation of a giant supramolecular porphyrin array by self-coordination. *Angew Chem. Int. Ed.* **39,** 4070–4073 (2000).
25. Hameren, R. V. *et al*. Macroscopic hierarchical surface patterning of porphyrin trimers via self-assembly and dewetting. *Science* **314,** 1433–1436 (2006).
26. Wang, Z., Medforth, C. J. & Shelnutt, J. A. Porphyrin nanotubes by ionic self-assembly. *J. Am. Chem. Soc.* **126,** 15954–15955 (2004).
27. Stupp, S. I. *et al*. Supramolecular materials: self-organized nanostructures. *Science* **276,** 384–389 (1997).
28. Hirschberg, J. H. K. K. *et al*. Helical self-assembled polymers from cooperative stacking of hydrogen-bonded pairs. *Nature* **407,** 167–170 (2000).
29. Rajendra, J., Baxendale, M., Rap, L. G. T. & Rodger, A. Flow linear dichroism to probe binding of aromatic molecules and DNA to single-walled carbon nanotubes. *J. Am. Chem. Soc.* **126,** 11182–11188 (2004).
30. Adachi, K. & Watarai, H. Two-phase Couette flow linear dichroism measurement of the shear-forced orientation of a palladium(II)-induced aggregate of thioether-derivatized subphthalocyanines at the toluene/glycerol interface. *New J. Chem.* **30,** 343–348 (2006).
31. Marrington, R. *et al*. Validation of new microvolume Couette flow linear dichroism cells. *Analyst* **130,** 1608–1616 (2005).
32. Yoshimura, T., Sakashita, H. & Wakabayashi, N. Real-time measurements of spatial velocity distribution with a laser Doppler imaging system. *Appl. Opt.* **22,** 2448–2452 (1983).
33. Yoshida, N., Aratani, N. & Osuka, A. Poly(zinc(II)-5,15-porphyrinylene) from silver(I)-promoted oxidation of zinc(II)-5,15-diarylporphyrins. *Chem. Commun.* 197–198 (2000).

Acknowledgements

The present work was sponsored by a Grant-in-Aid for Scientific Research (B) (no. 22350061) from the Ministry of Education, Science, Sports and Culture, Japan, by JST, Research Seeds Program, by Hyogo Science and Technology Association and by TEPCO Research Foundation.

Author contributions

A.T. conceived and directed the project, contributed to all experiments, and wrote the paper. Y.N. and R.W. performed syntheses and spectroscopic studies. Y.N. carried out characterization of aerial sound waves. N.I. carried out TEM measurements. T.A. directed the study and contributed to the execution of the experiments and interpretation of results.

Additional information

The authors declare no competing financial interests. Supplementary information and chemical compound information accompany this paper at www.nature.com/naturechemistry. Reprints and permission information is available online at http://npg.nature.com/reprintsandpermissions/. Correspondence and requests for materials should be addressed to A.T. and T.A.